Front. Phys. 13(5), 137804 (2018)
https://doi.org/10.1007/s11467-018-0772-4

RESEARCH ARTICLE

Molecular dynamics study of nanodroplet diffusion on smooth solid surfaces

Zhao-Xia Niu[1,2], **Tao Huang**[1,3], **Yong Chen**[1,2,†]

[1] *Center of Soft Matter Physics and its Applications, Beihang University, Beijing 100191, China*
[2] *School of Physics and Nuclear Energy Engineering, Beihang University, Beijing 100191, China*
[3] *Institute of Theoretical Physics, Lanzhou University, Lanzhou 730000, China*
Corresponding author. E-mail: [†] *ychen@buaa.edu.cn*
Received September 13, 2017; accepted February 28, 2018

We perform molecular dynamics simulations of Lennard–Jones particles in a canonical ensemble to study the diffusion of nanodroplets on smooth solid surfaces. Using the droplet-surface interaction to realize a hydrophilic or hydrophobic surface and calculating the mean square displacement of the center-of-mass of the nanodroplets, the random motion of nanodroplets could be characterized by short-time subdiffusion, intermediate-time superdiffusion, and long-time normal diffusion. The short-time subdiffusive exponent increases and almost reaches unity (normal diffusion) with decreasing droplet size or enhancing hydrophobicity. The diffusion coefficient of the droplet on hydrophobic surfaces is larger than that on hydrophilic surfaces.

Keywords nanodroplet, Brownian motion, surface diffusion

PACS numbers 78.67.Tf, 05.40.-a, 68.08.Bc

1 Introduction

The motion of droplets on surfaces is a widely observed phenomenon in daily life. At the microscopic scale, a larger number of similar phenomena governing surface diffusion are at work, such as the random motion of single molecules and clusters. During nucleation formation in droplet condensation, the nanoscopic droplet exhibits a random motion. The diffusion dynamics of nanodroplets on a surface is of great importance in many industrial applications, including the inkjet printing [1, 2], thermal management of micro-electronic devices [3, 4], fabrication of self-cleaning surfaces [5, 6], and design of miniaturized chemical reactors [7, 8]. Moreover, the characteristics of the surface diffusion of nanodroplets are strongly correlated with sessile droplet evaporation [9, 10], droplet coalescence [11], droplet spreading [12], and nano-material self-assembly [13].

Many studies have been performed regarding surface diffusion. Sancho *et al.* theoretically studied the anomalous diffusion behaviors of classical particles on a solid surface modeled by an underdamped Langevin equation with ordinary thermal noise [14]. Using a periodic or a random two-dimensional potential to describe the particle-surface interaction, the authors showed that the anomalous behavior is controlled by the friction coefficient and stress described by ordinary canonical Maxwell–Boltzmann statistics. Zhu *et al.* measured the surface self-diffusion of an organic glass, and suggested that surface diffusion is the primary mechanism of surface evolution for organic glasses at the micrometer to nanometer scales [15]. Through combining extensive single particle tracking microscopy data of endogenous lipid granules in living fission yeast cells with analytical results, Jeon *et al.* demonstrated that at short times the granules undergo subdiffusion according to the laws of continuous time random walk theory [16].

Previous work regarding surface diffusion was mainly concerned with the random motion of single molecules, clusters, and solid nanoparticles. The diffusion of single molecules plays an important role in a variety of phenomena, such as the molecular dynamics that govern the folding processes of proteins [17] and self-assembly of molecules into more complex materials [18]. The random motion of molecules can be modeled by solid nanoparticles where the motion on the surface is characterized by a combination of rolling, sliding, and sticking [19–22]. However, the surface diffusion of liquid droplets is more similar to the Brownian motion, even if sometimes

the droplet exhibits rolling and sliding behaviors [23–25]. This droplet diffusion behavior depends on the surface properties and temperature [24, 26]. This provides the possibility to control droplet motion by adjusting the gradient tension or wettability of substrate surfaces [24]. For smooth surfaces, the shape deformation of the droplet greatly influences its diffusion behavior as well as the temperature and surface energy. Recently, Li *et al.* used molecular dynamic (MD) simulations to examine the dependence of the diffusion coefficient on temperature [26], but there was little discussion of the diffusion characteristics.

In this study, the dynamics of nanodroplet movement on a smooth solid surface are studied by MD simulations in canonical (NVT) ensembles using the 12-6 Lennard–Jones potential to model the interactions between atoms in the system. The nanodroplet motion on smooth surfaces was found to exhibit short-time subdiffusion and undergoes an intermediate-time superdiffusion eventually resulting in long-time normal diffusion. These diffusion characteristics are independent of the surface wettability and droplet size.

This paper is organized as follows. In Section 2 the details regarding the simulation model and methods of calculating diffusion exponent and diffusion coefficient are presented. In Section 3, the main results of the study, including the temperature and size of nanodroplets, the diffusion exponent, and coefficient of nanodroplet movement, are shown. Finally, a brief discussion of the results and conclusions are presented in Section 4.

2 Model and methods

2.1 Model

In the MD simulations presented herein, the nanodroplet was placed on a smooth solid surface. The simulation box was set as a cubic box, where the bottom solid smooth substrate contained five-layer atoms with a face-center cubic (100) structure. Initially, the droplet was simple cubic (SC) and placed on the substrate.

The well-known Lennard–Jones (LJ) potential was used to model the interactions between the atoms in the simulations presenter herein,

$$u(r_{ij}) = 4\epsilon_{ab}\left[\left(\frac{\sigma_{ab}}{r_{ij}}\right)^{12} - \left(\frac{\sigma_{ab}}{r_{ij}}\right)^{6}\right], \quad (1)$$

where r_{ij} is the distance between the i-th and j-th atoms, σ_{ab} is the collision diameter, and ϵ_{ab} is the potential well. The subscript labels, a and b, represent the different atom types. Here, s and l are used to denote the atoms in the solid substrate and liquid droplet, respectively. The parameters of the nanodroplet are $\sigma_{ll} = 0.3405$ nm and $\epsilon_{ll} = 0.922$ kJ/mol, which describe the argon atom [9]. For the substrate atoms, $\sigma_{ss} = 0.4085$ nm and $\epsilon_{ss} = 9.22$ kJ/mol parameters were used.

For the simulations, we chose $\sigma^*_{ll} = \epsilon^*_{ll} = m^*_{ll} = 1$ to reduce all units and $m_{ll} = 6.63 \times 10^{-26}$ kg/mol was used as the mass of the nanodroplet atom. The reduced mass of the substrate atoms is $m^*_s = 10$. Therefore, $\sigma^*_{ss} = 1.2$ and $\sigma^*_{ls} = (\sigma^*_{ss} + \sigma^*_{ll})/2 = 1.1$ can be obtained. The reduced temperature unit is $T^* = k_B T/\epsilon_{ll} = 1$, which corresponds to 119.8 K, and the time unit is $\tau = \sqrt{m_l \sigma^2_{ll}/\epsilon_{ll}}$ corresponding to the real duration of 2 ps.

It is clear that the values of ϵ^*_{ls} represent the interaction between the nanodroplet and substrate, namely the wetting properties. When ϵ^*_{ls} approaches 1, the contact angle (CA) of the nanodroplets is far less than $\pi/2$, exhibiting hydrophilic properties. If ϵ^*_{ls} is close to 0, the surface is hydrophobic and the CA is much larger than $\pi/2$. In this study, two systems were used, smooth hydrophilic and hydrophobic substrates, which are denoted by sE7 ($\epsilon^*_{ls} = 0.7$) and sE4 ($\epsilon^*_{ls} = 0.4$), respectively. The initial atom numbers of the large and small nanodroplets N_0 were set as 4561 and 2070, respectively. Three simulation scenarios are presented in this study, $N_0 = 4561$ and 2070 for the sE7 configurations denoted by sE7-13 and sE7-10, respectively, and $N_0 = 4561$ for sE4 denoted by sE4-13.

The simulations were performed using the LAMMPS package with periodic boundary conditions [27]. The dimensions of the simulation box were $57 \times 57 \times 47.5\sigma_{ll}$ ($19.41 \times 19.41 \times 16.17$ nm) for sE7-13 and sE4-13, and $43.7 \times 43.7 \times 38\sigma_{ll}$ ($17.70 \times 17.70 \times 12.94$ nm) for sE7-10. The Norse-Hoover thermostat was applied to the substrate atoms to control the temperature with a coupling time of 0.25τ in the NVT ensemble performed in the simulations [28, 29]. The system temperature was set to 0.67 in the liquid-vapor coexistence region near the triple point temperature 0.68 [9, 10, 30, 31]. The time step used was 0.002τ (4 fs), and the cutoff distance for the LJ potentials was set to $3.5\sigma_{ll}$ (1.19 nm). The system reaches its equilibrium state after relaxation and contains three parts, the solid substrate, liquid nanodroplet, and argon gas.

2.2 Methods

To classify the diffusion behaviors of nanodroplets, the mean square displacement (MSD) of the different lag times from the trajectories of the center of mass (COM) of droplets were calculated. Usually, the MSD satisfies the power-law property as follows:

$$\langle [r(t) - r(0)]^2 \rangle = \langle \Delta r^2(t) \rangle \sim t^{\gamma}. \quad (2)$$

Here, $r(t)$ is the position of the COM of the nanodroplets at time t on the x–y plane and γ represents the dif-

fusion exponent. Normally, diffusion behavior can be classified into five types: subdiffusion ($\gamma < 1$), normal diffusion ($\gamma = 1$), superdiffusion ($1 < \gamma < 2$), ballistic diffusion ($\gamma = 2$), and super ballistic diffusion ($\gamma > 2$). In this study, the trajectory data of the COM of the nanodroplets was used to calculate the MSD and the diffusion exponents were obtained by fitting according to the formula described above. Subsequently, the diffusion types at the short, intermediate, and long delay times were evaluated.

Based on the MSD calculation in Eq. (2), the investigation of the diffusion coefficient is of importance. Similarly, considering the motion of the COM of the droplets in the two-dimensional x–y plane, its diffusion can be characterized in terms of the MSD,

$$\langle \Delta r^2(t) \rangle = \int r^2 P(r,t) \mathrm{d}r = 4 D_\gamma t^\gamma, \tag{3}$$

where $P(r,t)$ is the probability density function used to find the COM of nanodroplets at position r at time t and D_γ is the generalized diffusion coefficient. The D_γ value was calculated using a long-time limit in varied scenarios to study its dependence on surface properties.

3 Results

3.1 Temperature evolution and nanodroplet size

Initially, the droplet spread steadily and adopted a spherical-cap shape after a short relaxation time, as shown in Fig. 1. To measure the surface wettability with different interactions between the liquid droplet and solid substrate, the mean CA at equilibrium was calculated by cutting the droplet into 90 slices with widths of 2° around the central vertical z-axis and counting the CAs of each slice. The calculation of the contact radius (CR), which is the radius of the contact area, was performed simultaneously. For scenario sE7-13, the mean CA was

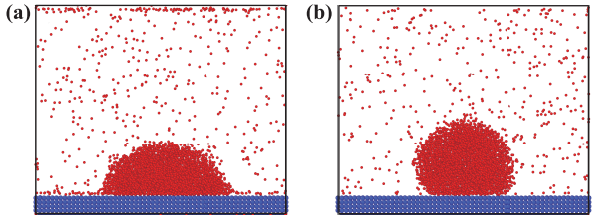

Fig. 1 The side views of nanodroplets on smooth solid **(a)** hydrophilic (sE7-13) and **(b)** hydrophobic (sE4-13) surfaces.

determined to be 76.90 ± 2.65 and mean CR was 13.48 ± 0.53 at $t = 900\ 000\tau$ [Fig. 1(a)]. Clearly the surface exhibits hydrophilic properties in sE7-13. Similarly, in Fig. 1(b), the mean CA is 118.75 ± 3.63 and mean CR is 9.74 ± 0.66 at $t = 500\ 000\tau$ in sE4-13, indicating that the substrate is hydrophobic. Furthermore, in the post-relaxation simulations, both the CA and CR for all three scenarios are stable with only minor fluctuation (The mean CAs are 118, 81, and 80.9 and mean CRs are 9.9, 13.5, and 10.2 for sE4-13, sE7-13, and sE7-10, respectively). The above calculation at a constant temperature shows that the solid surface becomes more wettable with larger droplet-surface interactions [26].

In the simulation, all scenarios were fixed at a constant reduced temperature $T^* = 0.67$ realized by the Norse-Hoover thermostat. Figure 2(a) shows the temperature evolution of the droplet in scenario sE7-13 over the entire simulation period ($2\ 000\ 000\tau$ or 4000 ns). A single scenario typically requires nearly one month of simulation in two optimized Intel Xeon E5-2680v3 CPUs. The droplet temperature clearly reaches a constant value very quickly and exhibits very small fluctuations (mean value of 0.67 with a standard deviation of 0.0089). Interestingly, the same temperature evolution was observed in the other two scenarios.

The initial SC argon atoms should form the liquid argon droplet and vapor due to thermal motion at the thermodynamic equilibrium after a short relaxation time (about 1300τ). Thus, the number of atoms in the droplet

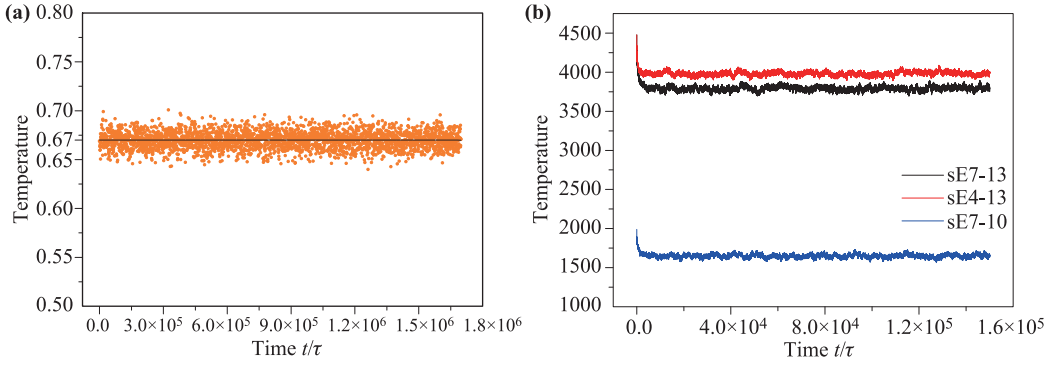

Fig. 2 The time evolutions of **(a)** the temperature of nanodroplet (sE7-13) and **(b)** the number of atoms in nanodroplets. The solid black line in panel (a) is the constant preset temperature $T^* = 0.67$ in all simulation scenarios.

at equilibrium is less than the preset number because of evaporation. Figure 2(b) shows the time evolution of the number of atoms in the droplets. For scenarios sE7-13 and sE4-13, the initial number of atoms (4561) reduced to the average values of 3792 and 3978, respectively. For sE7-10, the number of atoms is reduced from the initial 2070 to an average of 1649. Here, it should be noted that the droplet size of sE7-13 is smaller than that of sE4-13. This is because stronger droplet-substrate interactions result in a larger contact area with the substrate.

3.2 Nanodroplet diffusion

To study the motion of the nanodroplet on a solid smooth surface, the trajectory of the COM of the droplet was tracked in the x–y plane. As can be seen in Fig. 3 from 80 000τ (from time 600 000τ to 680 000τ) in scenario sE7-13, the random trajectory of the COM of the droplet is more similar to the Brownian motion of a colloid in suspension than the movement of a solid particle on a substrate which can roll and slide. A similar random motion phenomenon of the COM can also be observed in the simulations of scenarios sE4-13 and sE7-10 at equilibrium.

From the trajectory data of the COM of the nanodroplets, the MSD can easily be calculated $\langle \Delta r^2(t) \rangle$ as a function of delay time t. Figure 4 shows the log-log plots of the MSD for all scenarios at equilibrium over a large time range, spanning from the short- to long-time regimes. Upon examination of the reference line of normal diffusion (the solid black lines in Fig. 4), it is clear that the random motion of the droplets can be described as anomalous diffusion for short and intermediate times, which changes to normal diffusion at the long-time limit.

The measured MSD curves can be described by Eq. (2). Table 1 provides the values of the fitting slopes for the three time scales which are equal to the value of the diffusion exponent γ. For all three simulation scenarios, the droplet exhibits subdiffusion ($\gamma < 1$) behavior at short lag times ($t < 2\tau$) but normally diffuses ($\gamma = 1$) at long delay times ($t > 100\tau$). In the crossover region of lag-time scale, the droplet exhibits superdiffusion motion ($1 < \gamma < 2$). Note that the values of γ for the two hydrophilic cases (sE7) are nearly the same over the entire time scale. The diffusion exponent in sE4-13 is slightly larger than in scenario sE7. This indicates that the diffusion characteristics are primarily determined by the wettability of the solid surface and are independent of the size of droplets in these simulations.

Considering the long-time limit ($t \to \infty$), the diffusion exponent $\gamma = 1$ for all scenarios and long-time diffusion coefficient could be determined based on equation (3),

$$D_L = \lim_{t\to\infty} \langle \Delta r^2(t) \rangle / (4t). \tag{4}$$

Table 1 shows the D_L for the three simulations. It is clear that the diffusion coefficient is mainly determined by the wettability of the substrate (note that the temperature was held constant). The stronger interaction between the liquid droplet and solid surface ϵ_{ls} enhances the wettability and resulted in reduced diffusion motion. These results are consistent with previous theoretical and experimental studies which indicated that molecular surface diffusion and particle transport in fluids is mainly determined by the temperature and friction coefficient [26]. In the simulations adopting the NVT ensemble, the increasing ϵ_{ls} should enhance the friction at the interface and reduce the diffusion coefficient at a constant temperature.

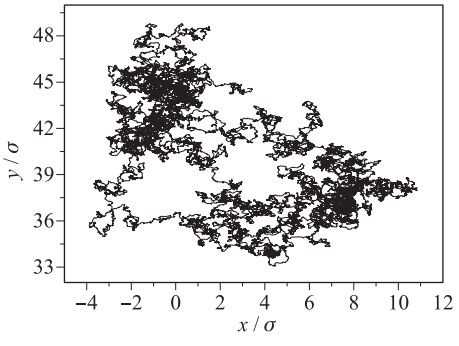

Fig. 3 The trajectory of the center of mass of nanodroplet (sE7-13) in x–y plane during 80 000τ. Note that the droplet crosses the left-side boundary along x-axis.

4 Conclusion and discussion

In this study, MD simulations in an NVT ensemble were performed to study the diffusion features of nanodroplets on smooth solid surfaces. To examine the effect of surface wettability on droplet motion, two droplet-surface interactions were used by adjusting the LJ parameter ϵ_{ls} to tune the surface properties, making them either hydrophobic or hydrophilic. Random motion of the nan-

Table 1 Diffusion exponents γ and long-time diffusion coefficients D_L of the nanodroplet on various smooth solid surfaces.

Scenario	Diffusion exponent γ			Diffusion
	Short-time	Intermediate-time	Long-time	coefficient D_L
sE4-13	0.8367	1.6335	1.0687	0.0040
sE7-13	0.7176	1.2227	0.9738	0.0011
sE7-10	0.7169	1.2241	0.9970	0.0013
sE7-8	0.7708	1.1551	1.0084	0.0016
sE7-7	0.8496	1.0657	1.0203	0.0023

odroplets was observed in all scenarios and follows the features of typical short-time subdiffusion, intermediate-time superdiffusion, and long-time normal diffusion. Interestingly, these diffusion characteristics are independent of the surface wettability. Two scenarios with smaller sizes were also examined: sE7-8 (droplet size 988) and sE7-7 (droplet size 457). As shown in Fig. 4 and Table 1, the decreased droplet size resulted in the short-time diffusive exponent approaching unity. This indicates that the diffusion of the sessile droplet becomes normal over all time scales.

Furthermore, it was observed that the long-time diffusion coefficient of the nanodroplet is principally governed by the surface wettability at a fixed temperature. Indeed, this dependence is consistent with previous reports [26]. In Fig. 4, the short-time diffusion coefficients are 0.0041 in sE7-10, 0.0020 in sE7-13, and 0.0016 in sE4-13. Thus, it can be concluded that in the short-time region, the size of droplets more significantly contributes to the diffusion coefficient.

Under the continuous-time random walk (CTRW) framework, in the short delay-time region, the awaiting-time distribution of the droplets exhibits a heavy tail [32]. Recently, Paul simulated the Rouse to reptation crossover in the motion of melt polymer chains using the bond fluctuation model [33]. The chains length in the bond-fluctuation model showed a clear indication of the first predicted crossover to $t^{1/2}$ behavior for the mean square COM displacement and to $t^{1/4}$ behavior for the mean square center monomer displacement. Herein, the characteristics of nanodroplet diffusion on smooth solid surfaces from short-time to long-time limits are presented. The simulated system appears simple but is actually quite complex. The above mentioned CTRW theory and the related reptation theory based on polymer diffusion may be helpful to more fully interpret the observations described herein in the future studies.

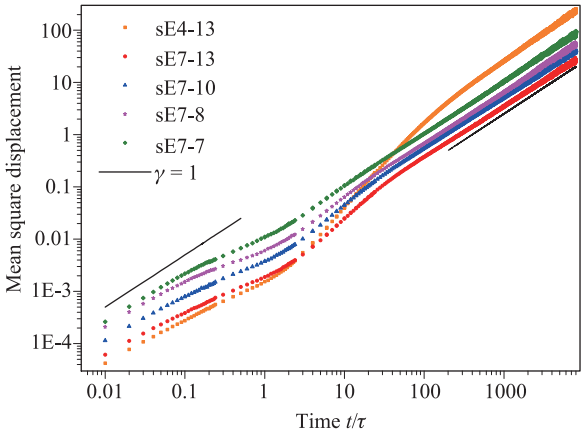

Fig. 4 Log-log plots of the MSD $\langle \Delta r^2(t) \rangle$ as a function of delay time t for three simulation scenarios. The black solid lines indicate the normal diffusion, $\langle \Delta r^2(t) \rangle \sim t$ with a slope of unity in the log-log plot.

Acknowledgements This work was supported by the National Natural Science Foundation of China under Grant Nos. 11675008 and 21434001.

References

1. H. Sirringhaus, T. Kawase, R. H. Friend, T. Shimoda, M. Inbasekaran, W. Wu, and E. P. Woo, High-resolution inkjet printing of all-polymer transistor circuits, *Science* 290(5499), 2123 (2000)
2. J. A. Lim, W. H. Lee, H. S. Lee, J. H. Lee, Y. D. Park, and K. Cho, Self-organization of ink-jet-printed triisopropylsilylethynyl pentacene via evaporation-induced flows in a drying droplet, *Adv. Funct. Mater.* 18(2), 229 (2008)
3. J. B. Boreyko and C. H. Chen, Self-propelled dropwise condensate on superhydrophobic surfaces, *Phys. Rev. Lett.* 103(18), 184501 (2009)
4. R. N. Leach, F. Stevens, S. C. Langford, and J. T. Dickinson, Dropwise condensation: Experiments and simulations of nucleation and growth of water drops in a cooling system, *Langmuir* 22(21), 8864 (2006)
5. R. Blossey, Self-cleaning surfaces — Virtual realities, *Nat. Mater.* 2(5), 301 (2003)
6. X. Deng, L. Mammen, H. J. Butt, and D. Vollmer, Candle soot as a template for a transparent robust superamphiphobic coating, *Science* 335(6064), 67 (2012)
7. X. Yao, H. Bai, J. Ju, D. Zhou, J. Li, H. Zhang, B. Yang, and L. Jiang, Running droplet of interfacial chemical reaction flow, *Soft Matter* 8(22), 5988 (2012)
8. A. Fallah-Araghi, K. Meguellati, J. C. Baret, A. E. Harrak, T. Mangeat, M. Karplus, S. Ladame, C. M. Marques, and A. D. Griffiths, Enhanced chemical synthesis at soft interfaces: A universal reaction-adsorption mechanism in microcompartments, *Phys. Rev. Lett.* 112(2), 028301 (2014)
9. Y. J. Sun, T. Huang, J. F. Zhao, and Y. Chen, Evaporation of a nanodroplet on a rough substrate, *Front. Phys.* 12(5), 126401 (2017)
10. J. Zhang, F. Leroy, and F. Müller-Plathe, Evaporation of nanodroplets on heated substrates: A molecular dynamics simulation study, *Langmuir* 29(31), 9770 (2013)
11. C. Andrieu, D. A. Beysens, V. S. Nikolayev, and Y. Pomeau, Coalescence of sessile drops, *J. Fluid Mech.* 453, 427 (2002)
12. N. Savva, S. Kalliadasis, and G. A. Pavliotis, Two-dimensional droplet spreading over random topographical substrates, *Phys. Rev. Lett.* 104(8), 084501 (2010)
13. N. Patra, B. Wang, and P. Král, Nanodroplet activated and guided folding of graphene nanostructures, *Nano Lett.* 9(11), 3766 (2009)

14. J. M. Sancho, A. M. Lacasta, K. Lindenberg, I. M. Sokolov, and A. H. Romero, Diffusion on a solid surface: Anomalous is normal, *Phys. Rev. Lett.* 92(25), 250601 (2004)
15. L. Zhu, C. W. Brian, S. F. Swallen, P. T. Straus, M. D. Ediger, and L. Yu, Surface self-diffusion of an organic glass, *Phys. Rev. Lett.* 106(25), 256103 (2011)
16. J. H. Jeon, V. Tejedor, S. Burov, E. Barkai, C. Selhuber-Unkel, K. Berg-Sørensen, L. Oddershede, and R. Metzler, *In Vivo* anomalous diffusion and weak ergodicity breaking of lipid granules, *Phys. Rev. Lett.* 106(4), 048103 (2011)
17. C. M. Dobson, Protein folding and misfolding, *Nature* 426(6968), 884 (2003)
18. G. M. Whitesides, J. P. Mathias, and C. T. Seto, Molecular self-assembly and nanochemistry: A chemical strategy for the synthesis of nanostructures, *Science* 254(5036), 1312 (1991)
19. S. Wang and Y. Zhu, Molecular diffusion on surface tethered polymer layers: Coupling of molecular thermal fluctuation and polymer chain dynamics, *Soft Matter* 6(19), 4661 (2010)
20. F. Klappenberger, Echoes from diffusion, *Nat. Mater.* 15(4), 374 (2016)
21. F. Celestini, Diffusion of a liquid nanoparticle on a disordered substrate, *Phys. Rev. B* 70(11), 115402 (2004)
22. G. D. Förster, F. Rabilloud, and F. Calvo, Adsorption of metal nanoparticles on carbon substrates and epitaxial graphene: Assessing models for dispersion forces, *Phys. Rev. B* 91, 245433 (2015)
23. T. A. Ho, D. V. Papavassiliou, L. L. Lee, and A. Striolo, Liquid water can slip on a hydrophilic surface, *Proc. Natl. Acad. Sci. USA* 108(39), 16170 (2011)
24. S. Daniel, M. K. Chaudhury, and J. C. Chen, Fast drop movements resulting from the phase change on a gradient surface, *Science* 291(5504), 633 (2001)
25. Z. Li and H. Wang, Drag force, diffusion coefficient, and electric mobility of small particles (I): Theory applicable to the free-molecule regime, *Phys. Rev. E* 68(6), 061206 (2003)
26. C. Li, J. Huang, and Z. Li, A relation for nanodroplet diffusion on smooth surfaces, *Sci. Rep.* 6, 26488 (2016)
27. S. Plimpton, Fast parallel algorithms for short-range molecular dynamics, *J. Comput. Phys.* 117(1), 1 (1995)
28. J. Davoodi, M. Safaralizade, and M. Yarifard, Molecular dynamics simulation of a gold nanodroplet in contact with graphene, *Mater. Lett.* 178, 205 (2016)
29. D. J. Evans and B. L. Holian, The Nose–Hoover thermostat, *J. Chem. Phys.* 83(8), 4069 (1985)
30. K. Yasuoka, M. Matsumoto, and Y. Kataoka, Evaporation and condensation at a liquid surface (I): Argon, *J. Chem. Phys.* 101(9), 7904 (1994)
31. K. Yasuoka and M. Matsumoto, Molecular dynamics of homogeneous nucleation in the vapor phase (I): Lennard-Jones fluid, *J. Chem. Phys.* 109(19), 8451 (1998)
32. N. Kumar, U. Harbola, and K. Lindenberg, Memory-induced anomalous dynamics: Emergence of diffusion, subdiffusion, and superdiffusion from a single random walk model, *Phys. Rev. E* 82(2), 021101 (2010)
33. W. Paul, Anomalous diffusion in polymer melts, *Chem. Phys.* 284(1–2), 59 (2002)